ADVANCED MATERIALS
www.advmat.de

Short Excited-State Lifetimes Mediate Charge-Recombination Losses in Organic Solar Cell Blends with Low Charge-Transfer Driving Force

Rishi Shivhare, Gareth John Moore, Andreas Hofacker, Sebastian Hutsch, Yufei Zhong, Mike Hambsch, Tim Erdmann, Anton Kiriy, Stefan C. B. Mannsfeld, Frank Ortmann, and Natalie Banerji**

A blend of a low-optical-gap diketopyrrolopyrrole polymer and a fullerene derivative, with near-zero driving force for electron transfer, is investigated. Using femtosecond transient absorption and electroabsorption spectroscopy, the charge transfer (CT) and recombination dynamics as well as the early-time transport are quantified. Electron transfer is ultrafast, consistent with a Marcus–Levich–Jortner description. However, significant charge recombination and unusually short excited (S_1) and CT state lifetimes (≈14 ps) are observed. At low S_1–CT offset, a short S_1 lifetime mediates charge recombination because: i) back-transfer from the CT to the S_1 state followed by S_1 recombination occurs and ii) additional S_1–CT hybridization decreases the CT lifetime. Both effects are confirmed by density functional theory calculations. In addition, relatively slow (tens of picoseconds) dissociation of charges from the CT state is observed, due to low local charge mobility. Simulations using a four-state kinetic model entailing the effects of energetic disorder reveal that the free charge yield can be increased from the observed 12% to 60% by increasing the S_1 and CT lifetimes to 150 ps. Alternatively, decreasing the interfacial CT state disorder while increasing bulk disorder of free charges enhances the yield to 65% in spite of the short lifetimes.

1. Introduction

Organic solar cells (OSCs) based on donor:acceptor blends have the potential to provide a cheap and carbon-neutral way of harvesting solar energy. Although, there has been a surge in efficiency of OSCs recently,[1–4] further improvement is important for commercial realization. In order to enhance the efficiency of these devices, the open circuit voltage (V_{OC}) and the short circuit current density (J_{SC}) need to be optimized. A common strategy to optimize the V_{OC} is to employ donor:acceptor blends with low driving force for interfacial charge transfer.[5,6] A low energetic offset between the frontier molecular orbitals of the donor and acceptor molecules results in the formation of an interfacial charge-transfer (CT) state with energy close to the singlet excited level of either the donor or the acceptor, which in turn results in an improved V_{OC} of the device. On the other hand, for such blends, Marcus theory predicts a slowdown of the electron transfer process due to the reduced driving force at the heterojunction, which could lead to recombination loss of the exciton population and lower photocurrent generation. Surprisingly, many of these donor:acceptor blends still simultaneously show high external quantum efficiency (EQE) and high V_{OC}, raising the following fundamental

Dr. R. Shivhare, G. J. Moore, Dr. Y. Zhong, Prof. N. Banerji
Department of Chemistry and Biochemistry
University of Bern
Freiestrasse 3, Bern CH-3012, Switzerland
E-mail: natalie.banerji@dcb.unibe.ch

A. Hofacker
Dresden Integrated Center for Applied Physics and Photonic Materials (IAPP) and Institute for Applied Physics
Technical University of Dresden
Nöthnitzerstrasse 61, D-01187 Dresden, Germany

The ORCID identification number(s) for the author(s) of this article can be found under https://doi.org/10.1002/adma.202101784.

DOI: 10.1002/adma.202101784

S. Hutsch, Prof. F. Ortmann
Department of Chemistry
Technical University of Munich
Lichtenbergstrasse 4, D-85748 Garching b. München, Germany
E-mail: frank.ortmann@tum.de

S. Hutsch, Dr. M. Hambsch, Prof. S. C. B. Mannsfeld, Prof. F. Ortmann
Center for Advancing Electronics Dresden
Technical University of Dresden
Helmholtzstrasse 18, D-01069 Dresden, Germany

Dr. T. Erdmann
IBM Almaden Research Center
650 Harry Road, San Jose, CA 95120, USA

Dr. A. Kiriy
Leibniz Institute of Polymer Research Dresden
Hohestrasse 6, D-01069 Dresden, Germany

questions: What mechanistic principles govern the charge-transfer process and subsequent dissociation of CT states in these low driving force blends?

Often, the charge-transfer process is explained within the framework of the classical Marcus formalism and its semi-classical variants, whereas the mechanism for the dissociation of CT states has been heavily debated.[7–9] The central question to be answered is how electron–hole pairs at the interface escape from their mutual Coulomb potential. Bässler and Köhler[10] suggest the formation of interfacial dipoles and delocalization of carriers as important parameters in overcoming the Coulomb barrier. On the other hand, work by Hood and Kassal[11] claims that the actual Coulomb barrier is of the order of k_BT at room temperature, owing to the presence of energetic disorder and due to entropic contributions to charge separation. Burke and McGeehee[12] have emphasized the importance of high local mobility at early timescales and energy cascades within the blend film. Specifically in the case of polymer:fullerene blends, the importance of fullerene cluster size and packing was highlighted by Jakowetz et al.[13] Larger fullerene clusters were shown to have higher density of band-like delocalized states, which once accessed could contribute to enhanced efficiency in charge carrier separation. Whether singlet excitons can effectively couple to such delocalized states in the absence of a significant driving force still remains an open question.

In the present study, we investigate a donor:acceptor blend consisting of a low-optical-gap diketopyrrolopyrrole (DPP) polymer: poly(3-([2,2″:5″,2‴:5‴,2⁗-terthiophen]-5-yl)-2,5-bis(6-dodecyloctadecyl)-2,5-dihydropyrrolo[3,4-c]pyrrole1,4-dione-6,5⁗-diyl), further referred to as P(DPP6DOT2-T), and the fullerene derivative PC[70]BM (see **Figure 1**a). We have adopted a multifaceted experimental and theoretical approach to study various factors affecting charge transfer and CT state dissociation in the P(DPP6DOT2-T):PC[70]BM blend. This blend exhibits a near-zero driving force (≈50–70 meV) for the interfacial electron transfer process, as evidenced by our earlier work.[14] We employ femtosecond transient absorption (TA) spectroscopy to quantify the singlet excited state (S_1) lifetime in pristine polymer films and the forward and backward electron transfer dynamics in DPP:PC[70]BM blend films. Then, CT state dissociation is studied using electromodulated differential absorption (EDA) spectroscopy. EDA spectroscopy enables us to track the separation of electron–hole pairs and their mobility dispersion at early timescales (<1 ns). On the theoretical side, we employ density functional theory (DFT) calculations to

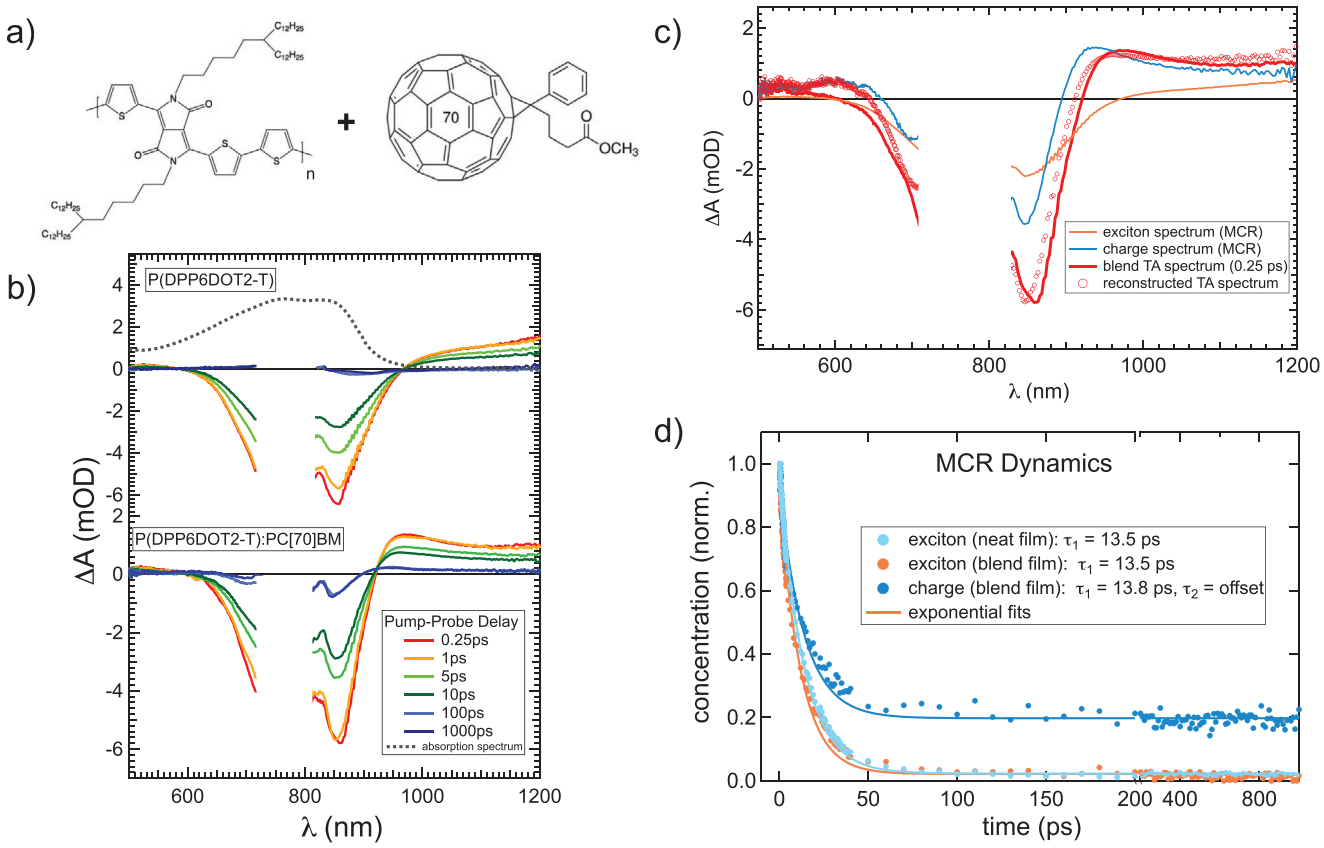

Figure 1. a) Chemical structure of the P(DPP6DOT2-T) polymer and the fullerene molecule PC[70]BM. b) Transient absorption (TA) spectra (λ_{pump} = 750 nm) for the pristine polymer P(DPP6DOT2-T) and the blend P(DPP6DOT2-T):PC70BM films at different pump–probe delay times. The absorption spectrum of the polymer film can be seen as the dotted line. c) Reconstruction of the early time (0.25 ps) TA spectrum of the blend film using the two components obtained from pure multivariate curve resolution (MCR) and their respective concentrations. The presence of the charge spectral component at early times verifies ultrafast electron transfer in this system. d) Temporal evolution of the exciton and the charge concentration profiles in the pristine and the blend film derived from MCR decomposition. Solid lines represent exponential fits.

compute transfer integrals for the electron transfer processes at the heterojunction. We also gain insights into electron–phonon coupling (EPC) by calculations of the mode-resolved reorganization energy. Using those parameters, the electron transfer rates are predicted within a modified semiclassical Marcus–Levich–Jortner (MLJ) framework and compared to the experimental values, as extracted from the TA data using a four-state kinetic model, that also allows to simulate the effect of bulk and interfacial disorder. Our main finding is that while interfacial electron transfer is still ultrafast at near-zero driving force, CT dissociation is relatively slow, leading to competing recombination channels mediated by a short S_1 excited state lifetime via S_1–CT electron back-transfer and hybridization.

We further demonstrate by means of simulations that the contribution of disorder is governed by the interplay of interfacial and of bulk disorder. While increased interfacial disorder might reduce the free charge (F) yield by slowing CT dissociation, increased bulk disorder can increase the yield by providing low-energy free charge states.

2. Results and Discussion

To probe the S_1 excited state lifetime and electron transfer dynamics, we carried out TA spectroscopy on the pristine polymer and the polymer:fullerene blend films. Figure 1b (top) shows the TA spectra of the pristine P(DPP6DOT2-T) film at various pump–probe delay times. Two major spectral bands can be identified: i) A negative differential absorption signal ($\Delta A < 0$) in the spectral range 600–950 nm, which corresponds to the ground state bleaching (GSB) and ii) a positive photoinduced absorption signal (PIA, $\Delta A > 0$) in the spectral range 950–1250 nm that can be ascribed to the excited state absorption (ESA).[15] The ESA signal primarily arises due to the absorption from the singlet S_1 state to higher-lying levels ($S_1 \rightarrow S_n$ transitions), since it completely vanishes at 100 ps. In the further analysis, we neglect any signal arising from triplet excitons (which might cause the weak long-lived GSB signature),[16] as their contribution to the differential absorption (ΔA) signal is very small in the temporal (0.1 ps $< t <$ 1200 ps) and spectral window (300 nm $< \lambda <$ 1200 nm) of our TA measurements. Thus, the decay of the ESA band corresponds to the S_1 lifetime, which is found to be 13.5 ps for P(DPP6DOT2-T) (see Figure 1d and Figure S1, Supporting Information). Surprisingly, compared to other conventional donor polymers,[17–19] the S_1 lifetime for this DPP polymer is about ≈20–30 times shorter (exciton-exciton annihilation can by excluded based on fluence-independent dynamics, Figure S3, Supporting Information). The reason for the short lifetime can be attributed to high non-radiative decay rates owing to the low optical gap ($E_{opt} \approx 1.33$ eV) of the polymer,[14] which is in accordance with the energy-gap law.[20] The validity of the energy-gap law in a variety of conjugated polymers (including DPP-based polymers) has been verified by Dimitrov et al.[17]

Figure 1b (bottom) shows the TA spectra of the blend film: P(DPP6DOT2-T):PC[70]BM, where we again see two main spectral features: The broad negative GSB signal and an extended PIA signal in the near-infrared (NIR) region. Comparing the spectra of the neat and blend films, we can clearly see a distinction between the positive spectral bands even at very early times (t = 0.25 ps). This suggests that some of the signal in the blend film already arises from charges, which can be either bound in the CT state or free, as this is undistinguishable by TA. To confirm this, we use multivariate curve resolution (MCR) to decompose the blend TA spectra into two contributions,[21] which we assign to pure "exciton" and "charge" (CT states + free charges) components (see Note S1, Supporting Information, for details). The "exciton" spectrum corresponds to the TA signature seen in pristine P(DPP6DOT2-T) film. The "charge" spectrum consists of the GSB, the electroabsorption signal due to the electric field around the photogenerated charges (causing the positive shoulder around 920 nm and blue-shifted GSB, see Figure S6, Supporting Information), as well as a broad PIA throughout the NIR range, similar to the polaron band seen when P(DPP6DOT2-T) is doped in the ground state (Figure S5, Supporting Information). After about 50 ps, only the "charge" spectrum persists in the TA data and gives rise to a long-lived offset. Figure 1c depicts the reconstruction of the early time (0.25 ps) TA spectrum of the blend film using the MCR components. Since we require the charge component to accurately reconstruct the TA spectrum, this verifies that electron transfer in the blend system happens on the ultrafast timescale (<200 fs). Using the extinction coefficient of the exciton absorption and absorbed photon density, we estimate that 60% of excitons dissociate to charges at early times. Ultrafast electron transfer in polymer:fullerene blends is an established phenomenon and has been commonly reported.[22,23] It is particularly noteworthy here that the negligible driving force in our blend ($\Delta E_{S1–CT} \approx$ 50–70 meV)[14] does not alter the rate of the charge transfer, as already previously observed for a few other systems.[24,25]

Figure 1d shows the MCR concentration dynamics of the exciton and charge components in the blend film. The lifetime of excitons that do not undergo ultrafast electron transfer is found to be 13.5 ps, which is identical to lifetime observed in the pristine polymer film. We also observe that about 80% of "charges" recombine with a time constant of 13.8 ps, which is comparable to the exciton decay time. Monomolecular (pump-intensity independent) charge recombination (Figure S4, Supporting Information) in OSCs is typically due to geminate charge recombination (gCR) of electron–hole pairs in the interfacial CT state.[26] However, gCR is generally much slower in other polymer:fullerene systems (hundreds of picoseconds to a few nanoseconds),[27,28] compared to the process seen here. Interestingly, for other DPP polymers, Dimitrov et al. reported similarly short lifetimes for the CT states using pump-push photocurrent spectroscopy,[29] which could be a consequence of the unusually fast recombination in these materials. The similar decay time of the CT and S_1 states (13–14 ps) suggests a correlation between their populations, caused by the low energetic offset between the two states. In the following, we will examine two ways in which the short-lived S_1 state of the polymer can mediate fast charge recombination in the P(DPP6DOT2-T):PC[70]BM blend. First, we consider electron back-transfer from the CT to the S_1 state followed by S_1 recombination ($CT \rightarrow S_1 \rightarrow S_0$). Second, a recent model by Brèdas et al.[30] suggests that there is mixing of the locally excited S_1 and the CT states, leading to the formation of a S_1–CT hybrid

state in low-offset donor:acceptor blends with strong electronic coupling between the states. This could increase the CT → S_0 recombination rate.

To theoretically predict the rates for the interfacial forward and backward electron transfer processes as well as the extent of S_1–CT hybridization, the relevant parameters (reorganization energies, transfer integrals between frontier molecular orbitals) were computed using DFT. A representative section of the P(DPP6DOT2-T) polymer chain (three monomer units with alkyl chains cut at the branching point) and the entire fullerene molecule was considered. The geometry of the oligomer:fullerene dimer was optimized at the B3LYP/3-21G** level of theory,[31,32] and the lowest energy dimer was considered to estimate the parameters. The transfer integral values ($\varepsilon_{\text{LUMO–LUMO}}$) varied between 20–40 meV and were strongly dependent on the relaxed geometry of the oligomer:fullerene dimer. Next, we studied the EPC for the P(DPP6DOT2-T):PC[70]BM dimer, which can be described in terms of the reorganization energy (Λ) for organic molecules.[33,34] In order to discern which vibrational modes of the oligomer:fullerene dimer contribute to the reorganization energy, we first map the cumulative reorganization energy ($\Lambda_{\text{DA}}(\omega)$) as a function of mode energy ($\hbar\omega$) in Figure 2a. The total reorganization energy for the dimer is of the order of 135 meV, which is on the lower side compared to other organic semiconductors. Second, we observe that mostly the high frequency vibrations significantly contribute to the total reorganization energy. The low reorganization energy combined with the contribution of mainly high frequency modes suggests that the DPP backbone motif is rigid and not susceptible to large structural modifications.

To calculate the interfacial electron transfer rates, we use the semiclassical MLJ framework. For accuracy of calculations, the concept of reduced reorganization energy (Λ'_{red}) is evoked.[35] This explicitly takes into account only the low-frequency modes ($\hbar\omega \leq 86$ meV) which effectively couple with the electronic motion, while all the high-frequency vibrations ($\hbar\omega > 86$ meV) are treated as a single effective mode. To further account for the fast nature of the electron transfer process, the slowest vibrations are treated quasi-statically (for more details refer to the Experimental Section). The Λ'_{red} for the P(DPP6DOT2-T):PC[70]BM dimer is of the order of ≈40 meV, which can be seen as the first saturation point in Figure 2a. Figure 2b depicts the electron transfer rate as a function of the S_1–CT state energetic offset ($\Delta E_{\text{S1–CT}} = E_{\text{S1}} - E_{\text{CT}}$) in logarithmic scale. The inset

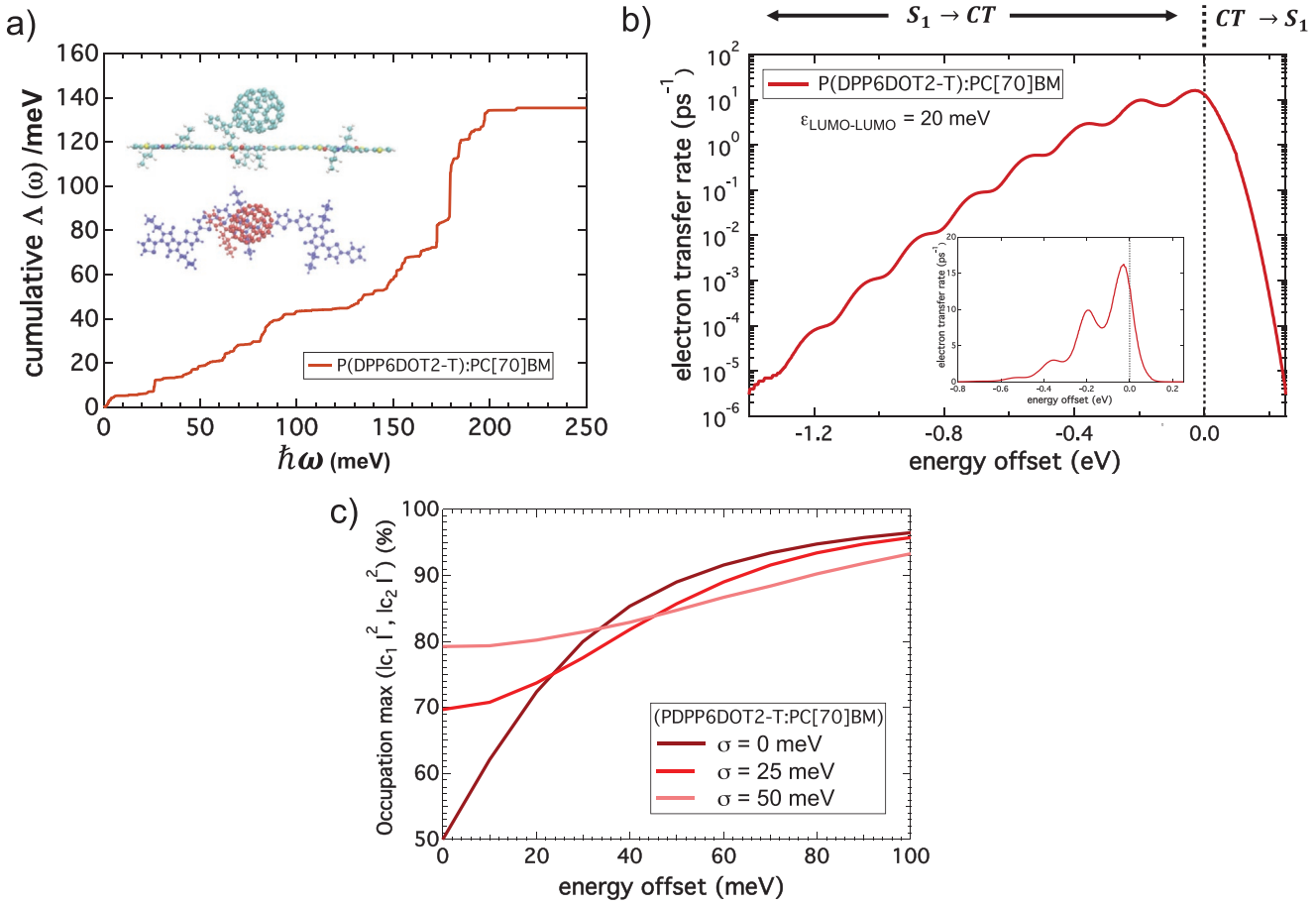

Figure 2. a) Mode-resolved reorganization energy $\Lambda_{\text{DA}}(\omega)$ for the oligomer:fullerene dimer representing P(DPP6DOT2-T):PC[70]BM. b) Electron transfer rate in logarithmic scale as a function of S_1–CT state offset for the oligomer:fullerene dimer calculated within the framework of Marcus–Levich–Jortner (MLJ) theory. A positive offset favors the S_1 → CT transition while a negative offset favors the back-transfer process: CT → S_1. The inset shows the transfer rate in linear scale. c) Effects of S_1–CT mixing ($\varepsilon_{\text{LUMO–LUMO}} = 20$ meV): Representation of the dominant component (S_1 or CT) in the hybridized eigenstates as a function of driving force and static disorder (σ).

shows the transfer rate in linear scale, revealing a distinct phonon-progression caused by the large vibronic coupling of the high-frequency modes.

At zero offset, the forward electron transfer rate is around 13 ps^{-1} which corresponds to an electron transfer time of ≈77 fs, in agreement with the ultrafast appearance of charges in the TA data. It is important to mention here that the quantum-chemical calculations represent the intrinsic charge-transfer rate but the experimentally observed rates can be lower because of the additional exciton diffusion step. It is noteworthy that the rate of electron transfer remains ultrafast here despite a near-zero driving force, which can be explained by the low reorganization energy of the rigid DPP system, so that maximum rates are predicted at negligible driving force. With a low $E_{S1} - E_{CT}$ offset of only 50 meV, we estimate a back-transfer time of 275 fs, opening a recombination channel via the short-lived S_1 state. Additionally, we also modeled CT → S_0 transition rates (Figure S7, Supporting Information) and find, in absence of any other recombination channel, a theoretical CT recombination time of ≈39 ns for the DPP:fullerene system studied here (with $E_{CT} \approx 1.33$ eV).[14]

Given that the frontier orbitals of the DPP polymer and the fullerene are nearly iso-energetic and have significant electronic coupling (20–40 meV), mixing of the orbitals can result in hybridized S_1–CT states. We estimate hybridization with a simple two state Hamiltonian, whose diagonalization yields new eigenstates and eigen-energies. This can be used to quantify the fraction of either S_1 or CT exciton in the possibly hybridized state (for more details refer to the Experimental Section). In Figure 2c we depict the dominant component (either S_1 or CT state) of the hybrid eigenstates as a function of the $E_{S1} - E_{CT}$ offset. At zero offset and in the absence of static disorder, we have a 50% contribution from each of the states representing a completely hybridized system. However, at finite driving force (≈50–70 meV) relevant for our system, the eigenstate has a more localized character ($|c_i|^2 >$ 80%). Additional localization occurs in the presence of inhomogeneous energetic disorder ($\sigma > 0$). At zero driving force, the CT character of a hybrid eigenstate progressively increases from 50% to nearly 80% in the presence of 50 meV static disorder. From this analysis, we conclude that about 5–20% of the S_1 state mixes into the CT state for the investigated P(DPP6DOT2-T):PC[70]BM blend. Such hybridization of S_1 and CT states can affect the steepness of the absorption onset[36] and has ambivalent effects on solar cell performance. On the one hand it can increase the radiative recombination rate of CT states due to intensity borrowing, thereby suppressing non-radiative voltage losses.[37] On the other hand, hybridization will lead to incomplete electron transfer which can suppress the charge generation yield of the device and promote interfacial charge recombination (see below).[38]

In order to extract the rates of the S_1 and CT state dynamics experimentally, we analyze the concentration profiles obtained by MCR decomposition of the TA data using a four-state kinetic model as shown in **Figure 3**a (see Note S2 and Figure S12, Supporting Information, for details). In agreement with the DFT calculations, we allow equilibration between the S_1 and CT states, since fast back-transfer is possible due to their low energetic offset. Recombination to the ground state occurs from both the S_1 and CT states and is in competition with CT state dissociation into free charges. We assume that free charges do not recombine within the 1 ns TA window (since no bimolecular processes are observed, Figure S4, Supporting Information). By fixing the S_1 lifetime to that measured for the neat polymer (13.5 ps) and using the forward and backward electron transfer rates from DFT calculations as initial guesses, we arrive at a very good fit to the experimental data (Figure 3b). The electron transfer (S_1 → CT) and the back-transfer (CT → S_1) times are found to be ≈240 and ≈415 fs, respectively, which is slightly slower than those predicted by MLJ theory. Experiment and theory are still fully consistent to each other, given that the experiment averages over more different local configurations.

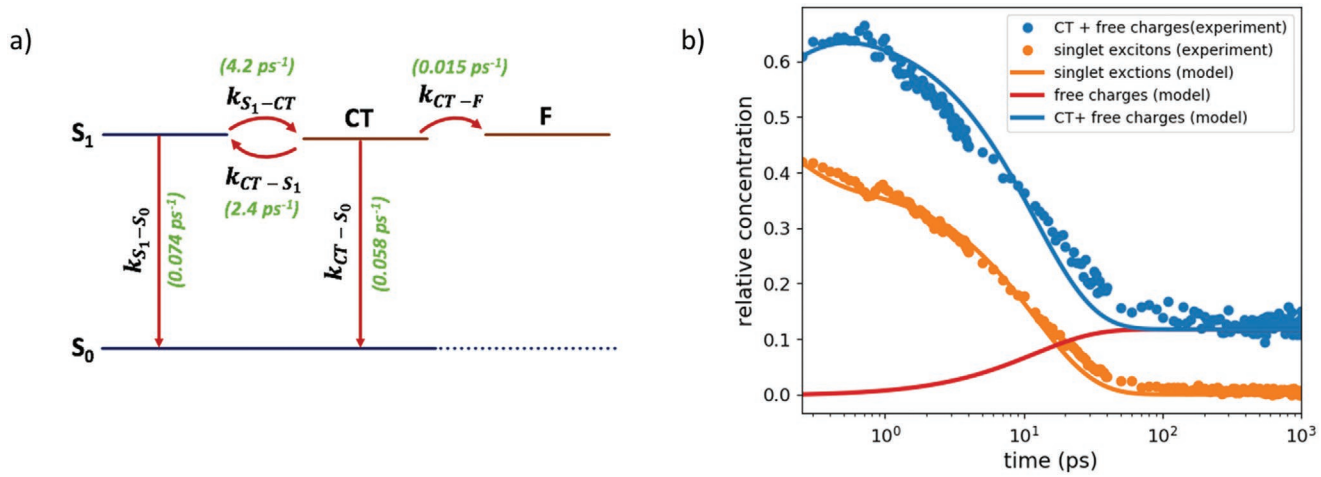

Figure 3. a) Jablonski diagram showing all the rate constants found by fitting the depicted four-state kinetic model to the experimental TA data. b) Experimental dynamics of the exciton and "charge" (CT state + free carrier (F)) populations obtained by MCR analysis of the TA data (markers), together with fits obtained from the four-state model (solid lines). A good fit with the experimental data was obtained. The concentrations are normalized by the total absorbed photon density (equal to the total charge plus exciton population at early times), after finding the initial exciton population based on the absorption coefficient at 750 nm.

The small ratio between the forward and backward transfers predicted by theory and measured experimentally reflects the small energetic driving force. Together with the DFT calculations, the kinetic fit to the experimental TA data confirms subpicosecond electron transfer dynamics as well as the establishment of an S_1–CT equilibrium that is shifted toward the CT state (higher forward than back-transfer rate), rather than incomplete quenching of the initial exciton population. The significant electron back-transfer to the S_1 state observed here also explains the relatively high photoluminescence that was reported earlier for this blend system.[14]

Another key finding is that the average CT dissociation rate (CT → F) is about 65 ps, which is orders of magnitude slower than the ultrafast (≈100 fs) free charge generation reported for typical polymer:fullerene blends.[27,39–41] Such slow CT state dissociation has nevertheless been observed for other systems with low driving force for charge transfer.[42,43] This suggests that an energetic S_1–CT offset is necessary for excitons to directly couple into delocalized states of fullerene clusters and enable prompt separation of electron–hole pairs. For low offset blends such as P(DPP6DOT2-T):PC[70]BM, other mechanisms involving high local charge mobility and disorder become more important (see below). A consequence of the relatively slow CT state dissociation is the competition with CT state recombination, which is aggravated by two factors in the investigated DPP system: First, the CT → S_0 relaxation time (≈17 ps) is unusually fast judging from the kinetic model fit of our TA data. Considering only the CT–S_0 energy gap, MLJ theory predicts a much slower recombination time on the order of a few tens of nanoseconds. The fast CT state decay is possibly related to its hybridization with the short-lived S_1 state, which results in a much higher oscillator strength for the CT → S_0 transition. Second, the CT → S_1 back-transfer offers an additional recombination channel via fast relaxation of the S_1 to the ground state. Overall, we observe significant loss of the exciton plus charge population on the 1 ns timescale, so that the yield of free charges is only 12%.

This finding corroborates very well with our previous study on the same system where we found that the EQE in the spectral region of polymer absorption is ≈12%.[14] The power conversion efficiency was found to be ≈3.1% with a J_{SC} of 7.3 mA cm^{-2} and a V_{OC} of ≈656 mV.[14] Within our kinetic model, increasing the recombination times of the S_1 and CT states to 150 ps while keeping all other parameters the same enhances the charge yield to 60% (Figure S13, Supporting Information), highlighting the significance of that loss mechanism. Unlike reported for other systems,[44,45] the important gCR in P(DPP6DOT2-T):PC[70]BM is not associated with a strong field-dependence of charge generation according to time-delayed collection field (TDCF) measurements.[14] We attribute this to the strong contribution of the neutral S_1 state via hybridization and electron back-transfer.

Since coherent coupling of excitonic states to free charge states of fullerene clusters is not operative for the low-offset blend investigated here, CT state dissociation relies on incoherent hopping of the separating charges, in competition with their recombination. Various groups have highlighted the importance of high local carrier mobility at early timescales for this process.[12,46,47] Here, we monitor the charge carrier transport at the picosecond timescale using a technique known as EDA spectroscopy. EDA spectroscopy relies on the principle of the Stark effect[48] and measures the temporal evolution of the electroabsorption signal generated from the bulk of the film in the presence of an externally applied reverse bias (Figure S8, Supporting Information). For a detailed description of the technique, the reader is referred to the work by Rhisse et al.[15] The main idea is that, as the photogenerated free charges are moving toward the electrodes, they shield the externally applied voltage which in turn results in the decay of electroabsorption signal. The decay in the electroabsorption signal can be converted to the picosecond-resolved voltage drop across the device. The technique is similar to time-resolved electric field induced second harmonic generation,[49] where one measures the drop in the second harmonic intensity as a result of the electric field shielding. **Figure 4**a represents the normalized voltage drop ($\Delta V/|V_{total}|$) dynamics, whereby a voltage drop of –1 corresponds to all photogenerated carriers being extracted (as determined from integrated photocurrent measurements). The first important observation is that the onset of the voltage drop emerges only around 15–20 ps, which corresponds to the time

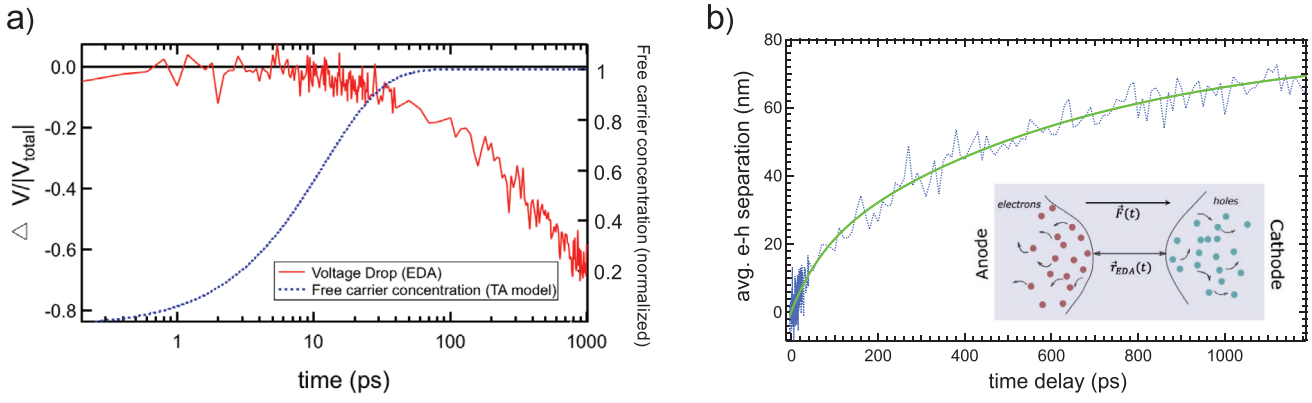

Figure 4. a) Voltage drop ($\Delta V/|V_{total}|$) dynamics extracted from the temporal decay of the electroabsorption signal and normalized by the total voltage drop obtained by an integrated photocurrent measurement. For comparison, the free charge concentration dynamics obtained from the kinetic modeling is shown. b) Average electron–hole (e–h) separation as a function of time. Inset: Schematic depicting the average spatial separation of an ensemble of electrons and holes.

at which CT state dissociation to free charges begins, in agreement with the slow (65 ps) CT state dissociation time found by modeling the TA data. This is in clear contrast to systems with higher driving force for charge transfer, where free charge generation and the EDA voltage drop are ultrafast (<100 fs).[15,50]

From the normalized voltage drop dynamics, the average electron–hole (e–h) separation, $\langle l(t)\rangle$, can be estimated according to the following relation:

$$\langle l(t)\rangle = \frac{\frac{\Delta V}{|V_{\text{total}}|}}{\frac{n_{\text{free}}(t)}{n_{\text{free}}(t=\infty)}} \times d \tag{1}$$

where d is the film thickness (225 nm) and $\frac{n_{\text{free}}(t)}{n_{\text{free}}(t=\infty)}$ is the temporal evolution of the free charge density normalized by their long-lived population density (offset), as extracted by fitting TA data with the kinetic model. The direct comparison of the TA data (un-biased films) with the EDA data (reverse-biased devices) is justified by the weak field-dependence of charge generation and extraction, as shown by our previous work using TDCF,[14] and confirmed by our integrated photocurrent measurements (Figure S9, Supporting Information). Figure 4b shows the evolution of the average e–h separation until 1 ns. It is important to mention that $\langle l(t)\rangle$ measured here refers to an average separation for an ensemble of electrons and holes projected along the axis joining two electrodes (schematically shown in the inset of Figure 4b). We observe an average e–h separation of around 20 nm on the 100 ps timescale which eventually increases to ≈60 nm on a nanosecond timescale.

From the gradient of $\langle l(t)\rangle$, we estimate the effective carrier mobility (μ_{EDA}):

$$\mu_{\text{EDA}} = \frac{d}{V}\frac{\partial\langle l(t)\rangle}{\partial t} \tag{2}$$

where V is the applied reverse bias voltage (6 V). On the 10 ps timescale, μ_{EDA} is around 10^{-1} cm^2 V^{-1} s^{-1} and gradually drops over a couple of orders of magnitude on the nanosecond timescale to $\mu_{\text{EDA}} \approx 7.5 \times 10^{-3}$ cm^2 V^{-1} s^{-1} at 1 ns (Figure S10, Supporting Information). When comparing to local mobility values obtained for other materials systems,[51–53] we observe that the early-time mobility that we find for the DPP:PC[70]BM system is on the lower side, which explains our finding of the slow CT state dissociation deduced via the kinetic model.

When considering different factors which determine the efficiency of CT-state dissociation, the role of energetic disorder has also been investigated by numerous groups, leading to conflicting reports.[11,25] To investigate the role of disorder, we expand our four-state kinetic model by extending each of the states to a Gaussian manifold of states (characterized by the standard deviation σ) and consider transitions between energy levels across the manifolds and within the manifolds, akin to a thermalization process (see **Figure 5**). Excited state lifetimes and the inter-manifold transition rates were adopted from the simple four-state kinetic model to the experimental TA data, to ensure that the new simulation captures similar parameter ranges. For energetic relaxation within the density of states (DOS) of each manifold we follow the Miller–Abrahams formalism.[54,55] For a detailed description of the model see Note S3 and Figure S14, Supporting Information.

In Figure 5a, we plot the external generation efficiency (EGE) surfaces as a function of interfacial disorder of CT states (σ_{CT}) and bulk disorder of free charges (σ_{free}). EGE is defined as the relative fraction of singlet excitations being converted to free carriers. In our simulations, we estimate EGE values by comparing the initial density of S_1 excitons to that of the free

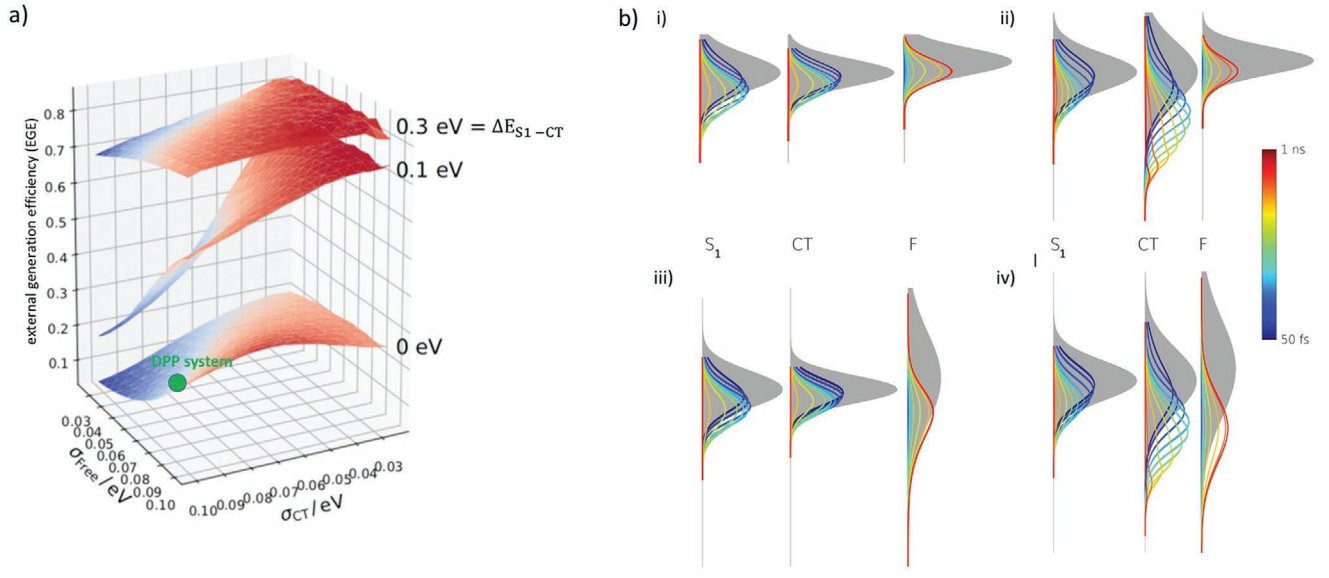

Figure 5. a) The simulated external generation efficiency (EGE) surfaces as a function of CT and free state disorder widths. The green dot represents the approximate position of the DPP system investigated in this paper. b) Simulated time evolution of density of occupied states (DOOS) distributions. Four representative cases for the zero-driving force scenario. For all cases, $\sigma_{S1} = 0.04$ eV, $\Delta E_{S1-CT} = 0$ eV and $\Delta E_{CT-F} = 0.025$ eV. i: $\sigma_{CT} = 0.03$ eV, $\sigma_F = 0.03$ eV, ii: $\sigma_{CT} = 0.065$ eV, $\sigma_F = 0.03$ eV, iii: $\sigma_{CT} = 0.03$ eV, $\sigma_F = 0.1$ eV, iv: $\sigma_{CT} = 0.065$ eV, $\sigma_F = 0.1$ eV.

carriers (F) after a nanosecond. The three surfaces correspond to three scenarios with different energetic offsets (ΔE_{S1-CT}). For the highest ΔE_{S1-CT} of 0.3 eV, the EGE is uniformly high and increases only slightly with increasing σ_{free} and decreasing σ_{CT}. The EGE surface at intermediate ΔE_{S1-CT} (0.1 eV) shows the same behavior but with much stronger amplitude: The EGE reaches values as low as 0.2 at high CT and low free state disorder. For the zero ΔE_{S1-CT} case, an interesting change happens: Decreasing the CT disorder width is not always beneficial for the EGE anymore. A maximum occurs around σ_{CT} = 0.07 eV, that shifts to lower σ_{CT} for lower σ_{free}. The reason is that singlet excitons that reside in the low energy tail of the singlet DOS have a lower probability of being promoted to the CT manifold if the CT states are located in a narrow distribution around the same central energy. Overall, these results suggest that high bulk (σ_{free}) disorder and low interfacial (σ_{CT}) disorder assist the dissociation of CT states. High bulk disorder ensures that electron–hole pairs can find favorable energetic configurations with increasing separation and diffuse beyond the Coulomb capture radius. This result is in agreement with the work of Kassal et al.,[11] where they suggest that the disorder is beneficial as it increases the entropy for charge separation. On the other hand, low σ_{CT} ensures that the CT excitons do not get trapped by relaxing into or starting out in lower-lying levels in the DOS. Similar conclusions were made by Menke et al.,[25] where they study the PIPCP:PCBM blend with low Urbach energies. These results unite the seemingly opposite views about the role of disorder by delineating the effects of the interfacial and bulk disorder.

Figure 5b depicts the time evolution (up to a ns) of the density of occupied states (DOOS) in the singlet, CT, and free carrier manifold. We consider four cases where the width of the singlet DOS is kept fixed while the relative widths of the CT and free carrier DOS are varied. These results confirm that high interfacial CT disorder leads to increased trapping: Even at short times, the majority of occupied CT states are situated at lower energies for the broad CT DOS cases, moving down further in energy as relaxation progresses toward the equilibration energy. The resulting energetic barrier slows down dissociation, analogously to dispersive recombination described in the previous work by Hofacker and Neher.[56] However, the effect is modified by the relative broadness of the S_1 and F manifolds: A large S_1 width enhances back-transfer and recombination, while a large F width enhances dissociation.

3. Conclusion

In this work, we have investigated a blend of a DPP polymer and the PC[70]BM fullerene derivative with a near-zero (≈50–70 meV) driving force for the electron transfer process. We have employed a series of complementary spectroscopic and theoretical tools to probe the sequence of events which ultimately leads to the formation of free charges. TA spectroscopy on the neat polymer film reveals a very short (≈13 ps) singlet exciton lifetime, likely due to high non-radiative recombination rates owing to the small optical gap of the DPP polymer (E_{opt} ≈ 1.33 eV). In the blend films, absorption signatures from CT states and/or free charges appear at early timescales (<0.2 ps), which validates the fact that electron transfer is ultrafast in this system. This finding is consistent with DFT calculations combined with MLJ simulations. Moreover, there is significant recombination in the blend films with a characteristic time constant of ≈14 ps, which is very similar to the exciton lifetime, suggesting that the S_1 and CT states are correlated. This hypothesis is validated by kinetic modeling of the TA data, where we observe a dynamic equilibrium between the S_1 and CT state populations. This equilibrium opens an additional recombination channel via the back-transfer process (CT → S_1 → S_0), representing one of the reasons for significant recombination in this blend system. Second, given the energetic proximity of the S_1 and CT levels, these states can hybridize as evidenced by theoretical calculations on a two-state model. Hybridization results in higher CT → S_0 recombination rates due to intensity-borrowing from the short-lived S_1 state, constituting a second reason for the observed fast recombination.

Another important result of the kinetic modeling is the relatively slow rise (≈65 ps) of the free charge population, which is not competitive with the fast CT state recombination. In the absence of a significant driving force, excitons cannot effectively couple to the delocalized states in fullerene clusters, causing this slow CT state dissociation. In such a scenario, incoherent hopping of Coulomb bound charges becomes the relevant process, which is governed by the short-range charge mobility. We use EDA spectroscopy to probe the local mobility in the P(DPP6DOT2-T):PC[70]BM system and find relatively low values at early times, which explains the slow CT state dissociation. In the last part of our study, we expand the kinetic model by including Gaussian manifolds of states in order to understand and generalize the effect of energetic disorder. We consider bulk disorder (σ_{free}) and interfacial (σ_{CT}) disorder separately to delineate their impact. The results suggest that a large σ_{free} and small σ_{CT} are beneficial for obtaining a high yield of free charges. Large σ_{free} implies a larger entropic contribution and thus a lower thermodynamic barrier for CT state dissociation, while a smaller σ_{CT} prevents the trapping of electron–hole pairs in low energy CT configurations where their dissociation is hindered.

In the broader context, our findings have important implications for non-fullerene acceptor (NFA)-based OSCs, as they frequently employ donor:acceptor combinations with low energetic offset to minimize voltage losses.[5,57–59] The model system investigated here highlights possible drawbacks that can limit the performance of such low driving force OPV blends. Two particular scenarios emerge in low energy offset systems: i) Establishment of an equilibrium between the S_1 state (also referred to as locally excited [LE] state) and the CT state populations, and ii) quantum mechanical mixing of the LE and CT states leading to the formation of hybridized states. A dynamic equilibrium between the LE and CT state populations has also been reported in NFA-based blends.[60–62] These reports highlight the positive effect of the equilibrium on non-radiative voltage losses ($\Delta V_{OC,\ non\text{-}rad}$). As the equilibrium shifts toward the LE states, $\Delta V_{OC,\ non\text{-}rad}$ substantially decreases due to the relatively high emission yield of the LE compared to the CT state.[63] The work by Eisner et al. suggests that the quantum mechanical mixing of LE and CT states leads to enhanced oscillator strength of the CT → S_0 transition due to intensity

borrowing,[37] again improving $\Delta V_{OC,non\text{-}rad}$ but possibly enhancing recombination. Our work clearly demonstrates the latter effect, as we observe important charge recombination, which is fostered by both the dynamic equilibrium and the hybridization, especially in the case of a short S_1 lifetime. This leads to significant loss of charges and thus limits the EQE and the efficiency of the device. Moreover, we show that CT state dissociation is slow in the absence of a significant energetic offset (tens of picoseconds timescale), making it difficult to compete with the fast recombination. Thus, long exciton lifetimes are essential in low offset systems to ensure a high yield of free charge generation, as is also highlighted in the recent work by Classen et al. for NFA-based blends.[60]

In addition, our work underlines the important role of local mobility in the dissociation of CT states via incoherent hopping. We are currently investigating by terahertz spectroscopy whether high local mobility in low energy offset NFA blends contributes to successful free charge generation. Finally, we generally show that efficient CT state dissociation also requires an optimized interplay of low interfacial and high bulk disorder. With regards to material design, the bulk disorder can be controlled by varying the polymer semicrystalline morphology, for example, via the architecture of the solubilizing alkyl sidechains. To reduce the interfacial disorder, donor:acceptor combinations with specific non-covalent interactions can be chosen, which leads to the ordering of the molecules at the interface. Solid-state NMR spectroscopy has proven to be a useful technique to study specific interfacial interactions,[64,65] and further investigations in this direction will be necessary. Overall, using a combination of ultrafast spectroscopy, quantum-chemical calculations, and simulations involving Gaussian manifold of states, we demonstrate that a long excited state lifetime, high local charge mobility, and fine-tuned interfacial/bulk disorder are key parameters to overcome recombination losses in low offset fullerene- or NFA-based OPV systems.

4. Experimental Section

Film and Device Preparation: The DPP polymer P(DPP6DOT2-T) was synthesized using a synthesis protocol reported earlier.[66] Fullerene derivative PC[70]BM was purchased from Ossila Ltd. and was used as received. The blend solution was prepared by dissolving the polymer and PC[70]BM in 1:3 ratio (weight/weight) using chloroform as the solvent. To obtain film thickness of around 200 nm, the solution was spin cast onto glass substrates at 2000 rpm for 60 s. To prepare solar cells for EDA measurements, the same solution was spin cast onto prepatterned indium tin oxide (ITO) substrates. The ITO substrates were functionalized with a thin layer (≈5 nm) of polyethyleneimine ethoxylated (PEIE). PEIE layer lowered the work function of ITO and made it suitable for electron collection. After spin coating the active layer, a combination of molybdenum oxide (MoO_3) ≈ 6 nm and silver (Ag) ≈ 100 nm was thermally evaporated for hole collection. Additionally, for doping the DPP polymer, the sequential deposition procedure was used. A solution of tris(4-bromophenyl) ammoniumyl hexachloroantimonate (also known as the "Magic Blue") in acetonitrile (≈1 mg mL^{-1}) was spin cast on top of a ≈100 nm thick neat P(DPP6DOT2-T) film at 2000 rpm for 45 s.

Transient Absorption and Electromodulated Differential Absorption Spectroscopy: TA and EDA spectroscopy are closely related and were performed on the same setup. Both the measurements were performed on a home-built setup using the output pulses from a regeneratively amplified Ti:sapphire laser system (Astrella from Coherent, 35 fs pulses at 800 nm with a frequency of 1 kHz and a pulse energy of 6 mJ). The output was split into two parts that ultimately generated the pump and the probe beams. The pump beam was frequency-converted to 750 nm with a commercial optical parametric amplifier (OPerA Solo, Coherent). The pump energy at the sample was adjusted to be in the linear regime of the TA response without any bimolecular artifact in the dynamics, which corresponded to a pulse energy of 50 nJ (where the absorption was weak, <0.1 OD). The pump pulse duration was about 60–80 fs (portable autocorrelator, pulseCheck, APE). The broadband "white light" probe beam was generated by focusing another portion of the fundamental laser output on a 5 mm sapphire plate. The probe was used to generate either a NIR continuum (830–1250 nm) or a visible continuum (500–730 nm) selected by using either 850 nm high pass or 750 nm low pass filters for removing the remaining 800 nm from the white light. The probe beam was split before the sample into a reference beam (to correct for laser intensity fluctuations) and a signal beam. The latter was then focused on the sample where it overlapped spatially and temporally with the pump pulses. The probe intensity was negligible compared to the pump intensity (probe energy of <5 nJ) and the spot size was much smaller allowing for a homogeneous excitation (probe diameter of ≈130 µm and pump diameter of ≈1100 µm, precisely determined for each measurement with a beam profiler, Thorlabs). The temporal delay between the two laser beams was achieved by varying the optical pathlength of the probe pulses with respect to the pump pulses using a computer-controlled delay stage (up to 1.5 ns). The visible and NIR parts of the TA spectra were recorded separately with two spectrographs, consisting each of a home-built prism spectrometer equipped with either two 512 × 58 pixel back-thinned Silicon CCDs (Hamamatsu S07030-0906) and or with two InGaAs arrays (Hamamatsu) for, respectively, visible and NIR detection of the signal and the reference beams. For the neat film, the TA spectra in the visible range were scaled to correct for a slightly weaker pump intensity. The spectrographs were assembled by Entwicklungsbüro Stresing, Berlin. Wavelength calibration was accomplished with a series of 10 nm bandpass filters. To improve sensitivity, the pump pulses were chopped at 500 Hz and the probe pulses were recorded shot-by-shot. The TA and EDA spectra were averaged until the appropriate signal-to-noise ratio was achieved (4000 shots per time delay, the whole four range of time delays was scanned 4–20 times). All the TA and EDA experiments were performed with a probe polarization at magic angle with respect to the one of the excitation beam to avoid effects of the polarization of the pump pulses on the probed absorption intensity. Also, along with the optical EDA measurements, the current response across the devices was recorded using a 50 Ω series load with a 400 MHz oscilloscope (Tektronix TDS 3044B). Prior to the data analysis, the spectra were corrected for the chirp of the white light, which was determined by measuring the pump–probe cross-correlation by the optical Kerr effect on a glass slide placed between crossed polarizers. This revealed a time resolution of about 70 fs.

Density Functional Theory Calculations and Simulations of Charge Transfer: Representative polymer:PC[70]BM dimers were obtained by performing geometry optimizations with DFT using the B3LYP functional,[67] 3-21G* basis sets,[68] and Grimme's DFT-D3 dispersion correction[69] as implemented in the Gaussian 16 package. The polymers were approximated by a chain of three monomer units and shortened alkyl side chains and were kept fixed during the relaxation. Different positions of PC[70]BM along the chain were screened and the relaxed structure of lowest energy was used as the representative geometry.

For this particular geometry, the charge-transfer rates between the CT and S_1 or S_0 state were calculated with a modified Levich–Jortner approach:

$$\upsilon(\Delta E) = \frac{2\pi}{\hbar}\varepsilon_{MN}^2 \frac{1}{\sqrt{4\pi\lambda_{therm}(T)k_BT}} \sum_k \frac{S_{eff}^k}{k!}\exp(-S_{eff})\exp\left(-\frac{\left(\Delta E + \Delta E_{qs} - \lambda_{red} - k\hbar\omega_{eff}\right)^2}{4\lambda_{therm}(T)k_BT}\right) \quad (3)$$

ε_{MN} are the electronic transfer integrals between the LUMO of PC[70]BM and the LUMO of the respective polymer or between the LUMO of PC[70]BM and the HOMO of the respective polymer. The transfer integrals were calculated with the fragment orbital approach[70] using the B3LYP functional,[67,71] 6-311G** basis set[72] with Gaussian 16.

The remaining contributions to $v(\Delta E)$ depended on the mode-resolved local EPCs g_M^i of mode i and molecule M. Here, M labeled either PC[70]BM or the respective polymer. The EPCs had been calculated as the derivatives of the Kohn–Sham energies of the LUMO or HOMO orbitals with respect to displacements along the normal modes.[32] They contributed to the reduced reorganization energy $\lambda_{red} = \sum_{M,i}^{lf} \hbar\omega_{M,i}(g_{M,i})^2$ and the thermal reorganization energy $\lambda_{therm}(T) = \sum_{M,i}^{lf} (\hbar\omega_{M,i})^2(g_{M,i})^2(1+2N_i)/(2k_BT)$ of the low-frequency dynamic modes. Further, they contributed to the EPC of the effective high-frequency mode $S_{eff} = \sum_{M,i}^{hf} (g_{M,i})^2$ and the energy difference ΔE_{qs} generated by the slow quasi-static modes, which followed a Gaussian distribution of $\sigma_{qs} = \left(\sum_{M,i}^{qs} (\hbar\omega_{M,i})^2(g_{M,i})^2(1+2N_{M,i}) \right)^{1/2}$. $\hbar\omega_{M,i}$ is the energy of mode i located at molecule M and $N_{M,i} = (\exp(\hbar\omega_{M,i}/(k_BT)) - 1)^{-1}$ was the respective thermal occupation following a Bose–Einstein distribution. The high-frequency modes contributing to the effective mode $\hbar\omega_{eff} = \frac{\sum_{M,i}^{hf} \hbar\omega_{M,i}(g_{M,i})^2}{\sum_{M,i}^{hf}(g_{M,i})^2}$ were separated from the remaining modes via a cut-off energy of 700 cm^{-1}. The slow quasi-static modes were defined via $\frac{\omega_{M,qs}}{\pi} < v(\Delta E)$ and were separated in a self-consistent fashion. The final transfer rate was obtained as an average over 5000 configurations of the quasi-static modes.

The degree of hybridization of the excitons was estimated within a simple two-state model. The states correspond to the local exciton (1) and CT-exciton (2). The energy difference between the two states, $\Delta\varepsilon = \varepsilon_2 - \varepsilon_1$, was generated by the driving force and additional energetic disorder. The coupling between the two states, ε_{12}, was the transfer integral between the LUMO of PC[70]BM and the LUMO of the respective polymer. Using these parameters, the two-state Hamiltonian was set up as

$$H_{2-state} = \begin{pmatrix} 0 & \varepsilon_{12} \\ \varepsilon_{21} & \Delta\varepsilon \end{pmatrix} \quad (4)$$

A subsequent diagonalization yielded the eigen energies and eigenstates $c = (c_1,c_2)$ and $d = (d_1,d_2)$. The square of the coefficients $|c_1|^2$ and $|c_2|^2$ measured the fraction of the basis states 1 and 2 in the new eigenstate c. If c was completely hybridized, which was the case for $\Delta\varepsilon = 0.0$, the coefficients evaluated to $|c_1|^2 = |c_2|^2 = 0.5$. For increasing disorder $\Delta\varepsilon$, the degree of hybridization decreased as shown in the main manuscript.

Supporting Information

Supporting Information is available from the Wiley Online Library or from the author.

Acknowledgements

R.S., G.J.M., Y.Z., and N.B. acknowledge the Swiss National Science Foundation (Grant 200020_184819) and the University of Bern for financial support. R.S. thanks the Center for Advancing Electronics Dresden for an INSPIRE grant allowing travel to Bern. S.H. would like to thank Studentenwerk Dresden for funding through the Saxony State Scholarship program. F.O. acknowledges the Deutsche Forschungsgemeinschaft (DFG) for funding through projects OR 349/1 and OR 349/3 and the cluster of excellence EXC 2089/1-390776260 (e-conversion). The authors thank the Zentrum für Informationsdienste und Hochleistungsrechnen of TU Dresden (ZIH) for grants of computing time.

Conflict of Interest

The authors declare no conflict of interest.

Data Availability Statement

The data that support the findings of this study are openly available in the Boris repository of the University of Bern (https://boris.unibe.ch/id/eprint/157186).

Keywords

charge transfer, energy materials, organic solar cells, photophysics, ultrafast spectroscopy

Received: March 5, 2021
Revised: June 18, 2021
Published online:

[1] B. Fan, D. Zhang, M. Li, W. Zhong, Z. Zeng, L. Ying, F. Huang, Y. Cao, *Sci. China: Chem.* **2019**, *62*, 746.
[2] S. Liu, J. Yuan, W. Deng, M. Luo, Y. Xie, Q. Liang, Y. Zou, Z. He, H. Wu, Y. Cao, *Nat. Photonics* **2020**, *14*, 300.
[3] J. Yuan, Y. Zhang, L. Zhou, G. Zhang, H.-L. Yip, T.-K. Lau, X. Lu, C. Zhu, H. Peng, P. A. Johnson, *Joule* **2019**, *3*, 1140.
[4] M. Zhang, L. Zhu, G. Zhou, T. Hao, C. Qiu, Z. Zhao, Q. Hu, B. W. Larson, H. Zhu, Z. Ma, *Nat. Commun.* **2021**, *12*, 309.
[5] J. Liu, S. Chen, D. Qian, B. Gautam, G. Yang, J. Zhao, J. Bergqvist, F. Zhang, W. Ma, H. Ade, *Nat. Energy* **2016**, *1*, 16089.
[6] K. Nakano, Y. Chen, B. Xiao, W. Han, J. Huang, H. Yoshida, E. Zhou, K. Tajima, *Nat. Commun.* **2019**, *10*, 2520.
[7] H. van Eersel, R. A. Janssen, M. Kemerink, *Adv. Funct. Mater.* **2012**, *22*, 2700.
[8] S. Few, J. M. Frost, J. Nelson, *Phys. Chem. Chem. Phys.* **2015**, *17*, 2311.
[9] S. Shoaee, M. Stolterfoht, D. Neher, *Adv. Energy Mater.* **2018**, *8*, 1703355.
[10] H. Bässler, A. Köhler, *Phys. Chem. Chem. Phys.* **2015**, *17*, 28451.
[11] S. N. Hood, I. Kassal, *J. Phys. Chem. Lett.* **2016**, *7*, 4495.
[12] T. M. Burke, M. D. McGehee, *Adv. Mater.* **2014**, *26*, 1923.
[13] A. C. Jakowetz, M. L. Böhm, J. Zhang, A. Sadhanala, S. Huettner, A. A. Bakulin, A. Rao, R. H. Friend, *J. Am. Chem. Soc.* **2016**, *138*, 11672.
[14] R. Shivhare, T. Erdmann, U. Hörmann, E. Collado-Fregoso, S. Zeiske, J. Benduhn, S. Ullbrich, R. Hübner, M. Hambsch, A. Kiriy, *Chem. Mater.* **2018**, *30*, 6801.
[15] J. De Jonghe-Risse, M. Scarongella, J. C. Brauer, E. Buchaca-Domingo, J.-E. Moser, N. Stingelin, N. Banerji, *Nat. Commun.* **2016**, *7*, 12556.
[16] J. R. Ochsmann, D. Chandran, D. W. Gehrig, H. Anwar, P. K. Madathil, K. S. Lee, F. Laquai, *Macromol. Rapid Commun.* **2015**, *36*, 1122.

[17] S. D. Dimitrov, B. C. Schroeder, C. B. Nielsen, H. Bronstein, Z. Fei, I. McCulloch, M. Heeney, J. R. Durrant, *Polymers* **2016**, *8*, 14.
[18] O. V. Kozlov, F. De Haan, R. A. Kerner, B. P. Rand, D. Cheyns, M. S. Pshenichnikov, *Phys. Rev. Lett.* **2016**, *116*, 057402.
[19] H. Kraus, M. C. Heiber, S. Väth, J. Kern, C. Deibel, A. Sperlich, V. Dyakonov, *Sci. Rep.* **2016**, *6*, 29158.
[20] R. Englman, J. Jortner, *Mol. Phys.* **1970**, *18*, 145.
[21] A. De Juan, J. Jaumot, R. Tauler, *Anal. Methods* **2014**, *6*, 4964.
[22] Y. Song, S. N. Clafton, R. D. Pensack, T. W. Kee, G. D. Scholes, *Nat. Commun.* **2014**, *5*, 4933.
[23] C. S. Ponseca Jr, P. Chabera, J. Uhlig, P. Persson, V. Sundstrom, *Chem. Rev.* **2017**, *117*, 10940.
[24] Y. Zhong, G. J. Moore, P. Krauspe, B. Xiao, F. Günther, J. Kublitski, R. Shivhare, J. Benduhn, E. BarOr, S. Mukherjee, *Nat. Commun.* **2020**, *11*, 833.
[25] S. M. Menke, A. Cheminal, P. Conaghan, N. A. Ran, N. C. Greehnam, G. C. Bazan, T.-Q. Nguyen, A. Rao, R. H. Friend, *Nat. Commun.* **2018**, *9*, 277.
[26] S. K. Pal, T. Kesti, M. Maiti, F. Zhang, O. Inganas, S. Hellstrom, M. R. Andersson, F. Oswald, F. Langa, T. Osterman, *J. Am. Chem. Soc.* **2010**, *132*, 12440.
[27] I. A. Howard, R. Mauer, M. Meister, F. Laquai, *J. Am. Chem. Soc.* **2010**, *132*, 14866.
[28] C. Dyer-Smith, I. A. Howard, C. Cabanetos, A. El Labban, P. M. Beaujuge, F. Laquai, *Adv. Energy Mater.* **2015**, *5*, 1401778.
[29] S. D. Dimitrov, A. A. Bakulin, C. B. Nielsen, B. C. Schroeder, J. Du, H. Bronstein, I. McCulloch, R. H. Friend, J. R. Durrant, *J. Am. Chem. Soc.* **2012**, *134*, 18189.
[30] X.-K. Chen, V. Coropceanu, J.-L. Brédas, *Nat. Commun.* **2018**, *9*, 5295.
[31] V. Coropceanu, J. Cornil, D. A. da Silva Filho, Y. Olivier, R. Silbey, J.-L. Brédas, *Chem. Rev.* **2007**, *107*, 926.
[32] F. Ortmann, K. S. Radke, A. Günther, D. Kasemann, K. Leo, G. Cuniberti, *Adv. Funct. Mater.* **2015**, *25*, 1933.
[33] Y. Li, Y. Yi, V. Coropceanu, J.-L. Brédas, *Phys. Rev. B* **2012**, *85*, 245201.
[34] A. Troisi, G. Orlandi, *Phys. Rev. Lett.* **2006**, *96*, 086601.
[35] K. Vandewal, J. Benduhn, K. S. Schellhammer, T. Vangerven, J. E. Rückert, F. Piersimoni, R. Scholz, O. Zeika, Y. Fan, S. Barlow, D. Neher, S. R. Marder, J. Manca, D. Spoltore, J. Cuniberti, F. Ortmann, *J. Am. Chem. Soc.* **2017**, *139*, 1699.
[36] M. Panhans, S. Hutsch, J. Benduhn, K. S. Schellhammer, V. C. Nikolis, T. Vangerven, K. Vandewal, F. Ortmann, *Nat. Commun.* **2020**, *11*, 1488.
[37] F. D. Eisner, M. Azzouzi, Z. Fei, X. Hou, T. D. Anthopoulos, T. J. S. Dennis, M. Heeney, J. Nelson, *J. Am. Chem. Soc.* **2019**, *141*, 6362.
[38] S. Few, J. M. Frost, J. Kirkpatrick, J. Nelson, *J. Phys. Chem. C* **2014**, *118*, 8253.
[39] S. M. Falke, C. A. Rozzi, D. Brida, M. Maiuri, M. Amato, E. Sommer, A. De Sio, A. Rubio, G. Cerullo, E. Molinari, *Science* **2014**, *344*, 1001.
[40] L. G. Kaake, C. Zhong, J. A. Love, I. Nagao, G. C. Bazan, T.-Q. Nguyen, F. Huang, Y. Cao, D. Moses, A. J. Heeger, *J. Phys. Chem. Lett.* **2014**, *5*, 2000.
[41] T. Unger, S. Wedler, F.-J. Kahle, U. Scherf, H. Bässler, A. Köhler, *J. Phys. Chem. C* **2017**, *121*, 22739.
[42] A. Devižis, J. De Jonghe-Risse, R. Hany, F. Nüesch, S. Jenatsch, V. Gulbinas, J.-E. Moser, *J. Am. Chem. Soc.* **2015**, *137*, 8192.
[43] D. A. Vithanage, A. B. Matheson, V. Pranculis, G. J. Hedley, S. J. Pearson, V. Gulbinas, I. D. Samuel, A. Ruseckas, *J. Phys. Chem. C* **2017**, *121*, 14060.
[44] S. Albrecht, S. Janietz, W. Schindler, J. Frisch, J. Kurpiers, J. Kniepert, S. Inal, P. Pingel, K. Fostiropoulos, N. Koch, *J. Am. Chem. Soc.* **2012**, *134*, 14932.
[45] J. Kurpiers, T. Ferron, S. Roland, M. Jakoby, T. Thiede, F. Jaiser, S. Albrecht, S. Janietz, B. A. Collins, I. A. Howard, *Nat. Commun.* **2018**, *9*, 2038.
[46] A. Devižis, K. Meerholz, D. Hertel, V. Gulbinas, *Chem. Phys. Lett.* **2010**, *498*, 302.
[47] D. Veldman, O. Ipek, S. C. Meskers, J. r. Sweelssen, M. M. Koetse, S. C. Veenstra, J. M. Kroon, S. S. van Bavel, J. Loos, R. A. Janssen, *J. Am. Chem. Soc.* **2008**, *130*, 7721.
[48] J. R. P. Angel, P. Sandars, *Proc. R. Soc. London, Ser. A* **1968**, *305*, 125.
[49] A. Devižis, A. Serbenta, K. Meerholz, D. Hertel, V. Gulbinas, *Phys. Rev. Lett.* **2009**, *103*, 027404.
[50] S. Gélinas, A. Rao, A. Kumar, S. L. Smith, A. W. Chin, J. Clark, T. S. van der Poll, G. C. Bazan, R. H. Friend, *Science* **2014**, *343*, 512.
[51] P. D. Cunningham, L. M. Hayden, *J. Phys. Chem. C* **2008**, *112*, 7928.
[52] M. J. Sher, J. A. Bartelt, T. M. Burke, A. Salleo, M. D. McGehee, A. M. Lindenberg, *Adv. Electron. Mater.* **2016**, *2*, 1500351.
[53] P. Krauspe, D. Tsokkou, E. Buchaca-Domingo, Z. Fei, M. Heeney, N. Stingelin, N. Banerji, *J. Mater. Chem. A* **2018**, *6*, 22301.
[54] A. Miller, E. Abrahams, *Phys. Rev.* **1960**, *120*, 745.
[55] S. Baranovskii, *Phys. Status Solidi B* **2014**, *251*, 487.
[56] A. Hofacker, D. Neher, *Phys. Rev. B* **2017**, *96*, 245204.
[57] G. Zhang, J. Zhao, P. C. Chow, K. Jiang, J. Zhang, Z. Zhu, J. Zhang, F. Huang, H. Yan, *Chem. Rev.* **2018**, *118*, 3447.
[58] J. Wang, J. Xu, N. Yao, D. Zhang, Z. Zheng, S. Xie, X. Zhang, F. Zhang, H. Zhou, C. Zhang, *J. Phys. Chem. Lett.* **2019**, *10*, 4110.
[59] S. Karuthedath, J. Gorenflot, Y. Firdaus, N. Chaturvedi, C. S. De Castro, G. T. Harrison, J. I. Khan, A. Markina, A. H. Balawi, T. A. D. Peña, *Nat. Mater.* **2021**, *20*, 378.
[60] A. Classen, C. L. Chochos, L. Lüer, V. G. Gregoriou, J. Wortmann, A. Osvet, K. Forberich, I. McCulloch, T. Heumüller, C. J. Brabec, *Nat. Energy* **2020**, *5*, 711.
[61] N. Gasparini, F. V. Camargo, S. Frühwald, T. Nagahara, A. Classen, S. Roland, A. Wadsworth, V. G. Gregoriou, C. L. Chochos, D. Neher, *Nat. Commun.* **2021**, *12*, 1772.
[62] G. Han, Y. Yi, *J. Phys. Chem. Lett.* **2019**, *10*, 2911.
[63] D. Qian, Z. Zheng, H. Yao, W. Tress, T. R. Hopper, S. Chen, S. Li, J. Liu, S. Chen, J. Zhang, *Nat. Mater.* **2018**, *17*, 703.
[64] A. Karki, J. Vollbrecht, A. L. Dixon, N. Schopp, M. Schrock, G. M. Reddy, T. Q. Nguyen, *Adv. Mater.* **2019**, *31*, 1903868.
[65] M. Seifrid, G. M. Reddy, B. F. Chmelka, G. C. Bazan, *Nat. Rev. Mater.* **2020**, *5*, 910.
[66] M. Hambsch, T. Erdmann, A. R. Chew, S. Bernstorff, A. Salleo, A. Kiriy, B. Voit, S. C. Mannsfeld, *J. Mater. Chem. C* **2019**, *7*, 3665.
[67] A. D. Becke, *Phys. Rev. A* **1988**, *38*, 3098.
[68] J. S. Binkley, J. A. Pople, W. J. Hehre, *J. Am. Chem. Soc.* **1980**, *102*, 939.
[69] S. Grimme, J. Antony, S. Ehrlich, H. Krieg, *J. Chem. Phys.* **2010**, *132*, 154104.
[70] B. Baumeier, J. Kirkpatrick, D. Andrienko, *Phys. Chem. Chem. Phys.* **2010**, *12*, 11103.
[71] A. D. Becke, *J. Chem. Phys.* **1993**, *98*, 1372.
[72] R. Krishnan, J. S. Binkley, R. Seeger, J. A. Pople, *J. Chem. Phys.* **1980**, *72*, 650.